Experimental and Theoretical Studies of the Lithium-fed Multichannel and Single-channel Hollow Cathode

IEPC-2005-094

Presented at the 29th International Electric Propulsion Conference, Princeton University October 31 – November 4, 2005

Leonard D. Cassady*and Edgar Y. Choueiri†
Electric Propulsion and Plasma Dynamics Laboratory (EPPDyL)
Mechanical and Aerospace Engineering Department
Princeton University, Princeton, New Jersey 08544

Cathode voltage and temperature profile measurements from lithium-fed single-channel hollow cathode (SCHC) and multichannel hollow cathode (MCHC) experiments are presented along with a the results of a theoretical model that includes the relevant phenomena. The lithium-fed SCHC experiments and the measurement of the plasma potential just downstream of the channel exit show that the plasma penetration length increases with current, and that the maximum temperature is independent of mass flow rate and weakly dependent on current (at high current). The model predicts important operating parameters including the cathode voltage, temperature profile, and ionization fraction as a function of current, lithium flow rate, and channel diameter. The SCHC model is also extended to a MCHC theory by including the thermal/radiative benefits of bundled channels. The theories capture experimental trends and predict cathode temperature to within 10% and voltage to within 4 V. One of the main insights provided by this study is that the arc penetrates to a location where the plasma density is great enough to supply the ion flux required to heat the cathode surface to the thermionic emission temperature. This has the effect of making the maximum temperature and voltage independent of mass flow rate and the penetration depth dependent on mass flow rate and current.

I. Introduction

High-power electric propulsion systems have long been recognized as among the most promising options for heavy-payload orbit raising and piloted planetary missions,[1–4] but research has been limited due to lack of in-space power. Among these high-power thrusters is the lithium Lorentz force accelerator (LiLFA), a type of magnetoplasmadynamic thruster (MPDT) that utilizes lithium propellant and a multichannel hollow cathode (MCHC). These features have been experimentally shown to improve the performance and lifetime of the LiLFA over a standard gas-fed MPDT,[5] but the fundamental operation of such a cathode configuration is poorly understood. The MCHC is critical to the LiLFA due to its dual purpose role of plasma source and arc cathode, yet there is no model that describes its operation. Therefore the motivation of this research is to develop an understanding of the fundamental physics of the MCHC with lithium vapor propellant in order to enhance the performance of the LiLFA.

No complete MCHC model has been previously presented, although Declroix *et al.* demonstrated through experiments and analysis[6] that the division of mass flow rate and current between channels can reduce discharge voltage and cathode temperature. However, for a more detailed and predictive model, we must base our theoretical analysis on a similar cathode (the SCHC), on which more work has been accomplished. Ferreira and Delcroix[7] presented the most detailed theory of the SCHC, however it required experimental

*Research Assistant, Mechanical and Aerospace Engineering Department, lcassady@princeton.edu, AIAA student member
†Chief Scientist, EPPDyL. Associate Professor, Applied Physics Group, Mechanical and Aerospace Engineering Department, choueiri@princeton.edu.

data (the cathode temperature profile) as an input and was applicable only to argon-fed devices. In this paper, we present the results from predictive SCHC and MCHC models that do not require experimental data as an input, but rather only for validation. The development of an accurate hollow cathode model has been limited by the lack of experimental data to validate the theory. Of the few experiments that utilized a lithium-fed SCHC or MCHC,[5,8–12] most focused on thruster operation instead of the cathode. In fact, we do not know of any published measurements of the cathode voltage (rather than the total discharge voltage) in a lithium-fed cathode. The temperature profile of an MCHC had been measured at a few conditions,[8,9] but not enough data exist to allow the determination of trends in the dependence of the cathode voltage, the temperature and plasma penetration depth on the operating parameters.

We present here the results of lithium-fed SCHC and MCHC experiments that reveal such trends as well as a theoretical model that includes the relevant physical processes with the aim of combining theory and experiments to extract lacking physical insight into the nature of the controlling processes.

We first present an overview of the SCHC and MCHC in section II. A theory of their operation, which is an improved version of that presented earlier by Cassady and Choueiri,[13] is summarized in section III. In sections IV and V we describe the apparatus and diagnostics, respectively, designed to validate the theory. The experimental data are presented and discussed in section VI, followed by a comparison to theoretical predictions in section VII.

II. The Multichannel and Single-channel Hollow Cathode

Multichannel hollow cathodes conduct high currents at low voltage while having longer lifetime than other cathodes operating at similar conditions. They differ from planar or solid cathodes in that they have many channels that are open to the plasma in the inter-electrode space, as shown in figure 1. Most hollow cathodes operate with gas flow through the channels into the discharge volume. The plasma penetrates the cavities under many operating conditions, and that allows the arc to attach to the cathode in a confined volume. As described in detail below, the geometry of the channels maintains a dense, highly ionized plasma near the cathode surface and thus more effectively allows a high current (10s to 100s A) to be conducted from the plasma to the material.

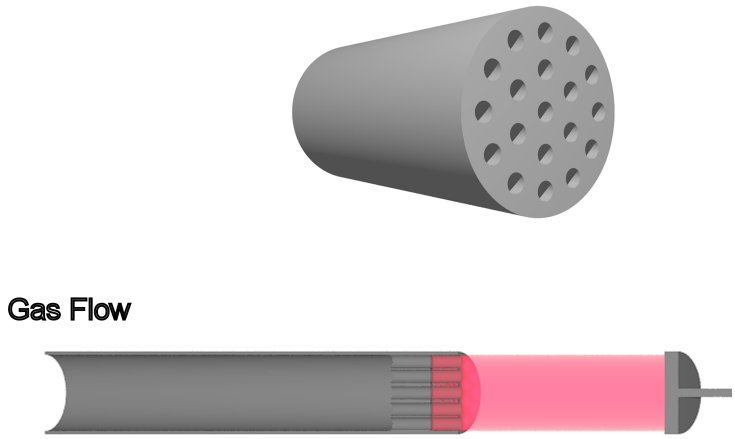

Figure 1. Schematic of the MCHC. The top image is an isometric of a 19 channel cathode. The bottom image is a cut-away view with the cathode on the left, anode on the right, and the plasma shown penetrating the channels.

Since an MCHC consists of many parallel channels working together, we will first explain how each channel operates. Each channel is similar to a single-channel hollow cathode (SCHC), which is better understood and provides a basis for our research, although no complete model has been previously developed. Physically,

an SCHC is a thin-walled (0.01-1 mm) tube of refractory metal (tantalum or tungsten). At pressures below 0.1 Torr in the inter-electrode space, the anode location and background pressure do not affect the operation of the cathode. The working gas is introduced through the channel of the cathode where a relatively high pressure (a few Torr) is created because the flow is choked as it exits into the inter-electrode space. The arc attaches to the interior surface of the channel at a distance from the tip that depends on the value of mass flow rate divided by the cross-sectional area of the channel, current, and heat conduction axially along the cathode.

Delcroix *et al.* developed the multichannel hollow cathode to allow for greater current at a wide range of mass flow rate.[6] The MCHC was simply conceived as a grouping of many SCHCs in the same cathode. They demonstrated that the MCHC indeed delivered more current while maintaining a lower cathode voltage. Although no detailed theory was presented, they demonstrated that the division of mass flow rate and current between channels reduces the voltage and cathode temperature. This can be attributed to each channel being operated closer to the optimal density, the increase in surface area for the arc to attach to, and to the reduced thermal radiation lost from each channel.

The controllable parameters of a hollow cathode arc discharge are the channel diameter and length, the cathode wall thickness and material, the gas mass flow rate and type, and the current. The discharge adjusts the voltage of the cathode relative to the plasma in the external discharge, the temperature profile of the cathode (including the distance the plasma penetrates), the ionization fraction of the gas within the channel, and the electron temperature inside the channel, to provide the current demanded by the external circuit.

III. Lithium-fed Hollow Cathode Model Overview

An MCHC model requires an SCHC model and the inclusion of the thermal interaction of adjacent channels, and the division of current and mass flow. In fact, there is no published multichannel model that consistently includes ionization and current conduction. Ogarkov *et al.*[14,15] studied MCHC design by focusing on plasma-surface interactions. The seminal work on MCHCs by Delcroix, Minoo, and Trindade[6] presented no detailed theory, instead their insightful analysis compares MCHC operation to that of an SCHC.

Ferreira and Delcroix present the most detailed theory of the SCHC,[7] however, as we said above, it required experimental data (the cathode temperature profile) as an input and was applicable only to argon-fed devices. Our goal is to develop a self-consistent SCHC model that will not require experimental data as an input, but rather that the predictions of the model can be compared to experimental data. To attain that goal, we include a model of non-equilibrium ionization and excitation via thermionic and thermal electron collisions that utilizes a rate balance of the important excitation states of the neutrals. Here we present an overview of the SCHC model, since the details can be found in an earlier model.[13] We then extend our lithium-fed SCHC model to an MCHC model.

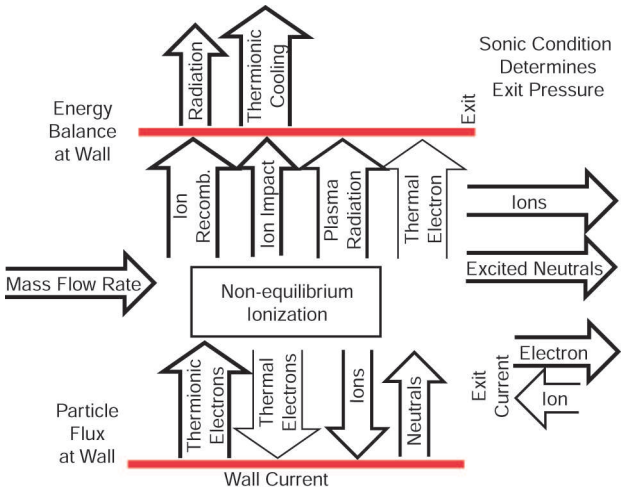

Figure 2. Diagram of some of the processes in included in the SCHC model: the particle flux balance at the wall and through the channel, the energy balance at the wall, current conduction, and the ionization process.

Our model predicts the measurable properties of the cathode during operation as a function of the controllable parameters: the channel diameter, propellant mass flow rate, and current. The relevant measurable properties that our model will predict are the cathode voltage and cathode temperature. A realistic physical model of the SCHC requires the inclusion of at least the following processes (shown in figure 2),

- Gas flow through the channel
- Non-equilibrium excitation/ionization
- Thermionic electron energy loss
- Work function reduction due to plasma sheath
- Current conduction at cathode
- Cathode heating
- Plasma electron heating

The channel of the hollow cathode is modelled as a cylinder of length l and radius r, shown in figure 3, within which the plasma properties are assumed uniform. The radius is an independent parameter that we choose according to experiments. We assume that the thermionic electrons are emitted from a uniform temperature tungsten wall that surrounds the channel. The number densities of the excited states of lithium and the thermionic electrons are determined by a rate balance of all of the collision and flow processes, assuming steady state.

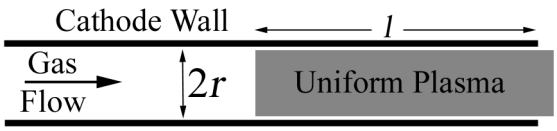

Figure 3. Schematic of the cylindrical SCHC adopted for the model.

A. MCHC Theory

An MCHC is essentially many SCHCs bundled together. The channels share walls for thermal radiation and conduction because of their proximity. Therefore, the MCHC model must account for thermal processes differently then in the SCHC model. The MCHC model also assumes that all of the channels have the same diameter, conduct the same current, and have the same mass flow rate. Hence, the mass flow rate and current in each channel is the total current and mass flow rate divided by the number of channels.

In an effort to keep a simple, yet effective model of the MCHC discharge, the thermal radiation and conduction will be equally apportioned to each channel. This technique may not be the most accurate model of thermal effects because the channels at the center of the cathode radiate heat into adjacent channels that are of the same temperature, so no heat can be exchanged. Also, the channels on the outer edge have a portion of their surface exposed to the external environment and thus lose some heat via radiation. We will assume that all channels contribute equally to the thermal radiation and that the total radiation area is only the exposed outer surface of the cathode. Similarly we will assume that each channel equally contributes thermal conduction power to the base of the cathode.

The area of an SCHC that contributes to thermal radiation is equal to the exposed outer surface of the cathode

$$A_{S,e} = 2\pi r_{ch} l. \tag{1}$$

The same is true for the MCHC, except the radius is determined by the outer diameter of the entire cathode

$$A_{M,e} = 2\pi r_{M,o} l, \tag{2}$$

where the $r_{M,o}$ is the outer radius of the MCHC. This area is not directly related to the individual channel radius ($r_{M,i}$) because the distance between channels and the hole pattern can be chosen independently.

Thus, we must formulate the power lost via thermal radiation differently for the MCHC model. The model decouples the radiation area from the individual channel radius. Each channel contributes equal portions to the exposed area of the MCHC,

$$A_{eff} = \frac{A_{M,e}}{N}, \tag{3}$$

where N is the number of channels in the cathode. Similarly, we average the power loss via conduction to the cathode base over all of the channels.

The MCHC model solves for the operation of a single channel using the SCHC formulation except for exchanging the exposed area with A_{eff}. Because each channel has an identical mass flow rate, current, and thermal power loss, we only have to solve a model of a single channel.

To demonstrate the advantage of the MCHC, we give an example of the reduction in thermal radiation power loss as compared to the SCHC. With 2 concentric rings of holes around a central hole, 19 holes can fit in a tight pattern. The radius, $r_{M,o}$, is approximately 4 times the radius of channels, which also increases the exposed area by a factor of 4. Yet there are 19 channels within the cathode providing heat to the surface area. The effective surface area will be $\frac{4}{19}$ or 21% of the area an SCHC would have. Since the radiated power is directly proportional to area, there is a 79% reduction in that power loss mechanism, which is dominant at low current and significant at medium current.[13]

IV. Apparatus

This section describes the components of the lithium-fed hollow cathode experimental apparatus. The experiments were conducted in lithium experimental facility (LEF) at the Electric Propulsion and Plasma Dynamics Laboratory. The facility is configured to operate with lithium and high temperature components. The primary components of the experimental apparatus are the cathode, anode, lithium feed system, lithium evaporator, vacuum facility, and the apparatus that maintains optical access. The general layout is illustrated in figure 4.

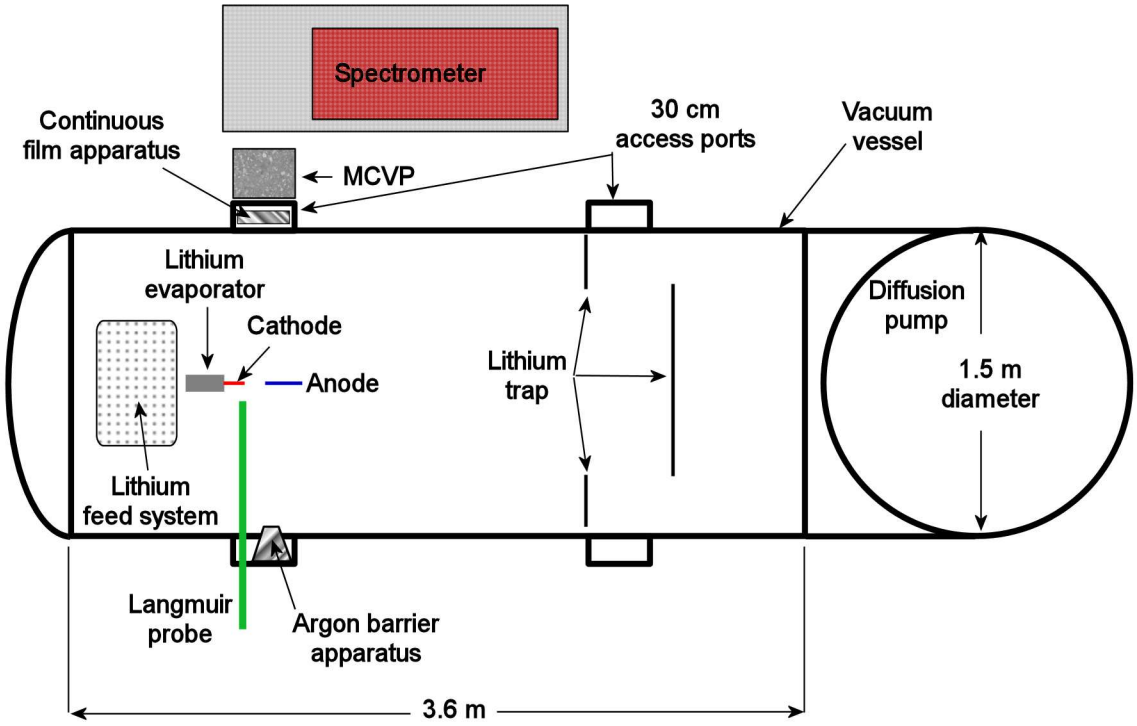

Figure 4. General Facility Layout of the LEF

The cathode was located near the vertical and horizontal centers of the cylindrically-shaped facility at the axial location of the 30 cm access ports. This location allowed optical access for the multi-color

video pyrometer (MCVP) and spectrometer, as well as physical access with the Langmuir probe. The two apparatus designed to maintain optical access were located on the access ports near the cathode, one on each side. The MCVP and spectrometer utilized the same port, so the MCVP was removed when spectroscopy data were acquired. The feed system and vacuum facility are discussed in Kodys, Emsellem, Cassady, Polk, and Choueiri.[16]

A. Electrode Set-up

The anode was located approximately 3 cm from the cathode, and aligned with the cathode axis. An experiment accomplished at EPPDyL, as well as by previous researchers,[6] demonstrated that the location of the anode has little effect on the cathode portion of the discharge. The anode was a 3/4" (1.9 mm) diameter tungsten rod with a spherical tip. Its stainless steel support was water-cooled during high-current experiments.

B. Cathode Specifications

Three cathodes were designed and built specifically to explore the operation of lithium-fed hollow cathodes. The goal was to create cathodes that were the easiest to physically model, diagnose, and exchange. The cathode affects the discharge through its thermionic electron emission and thermal radiation properties and through thermal conduction away from the discharge. The first two properties are inherent to the material choice, which are practically limited to tungsten for these experiments. The cathode wall thickness was reduced as much as possible and the length made as long as possible to reduce thermal conduction effects.

1. SCHC Dimensions

The cathode length and the wall thickness can play an important role in the discharge because thermal conduction from the attachment region can be affected by those dimensions. The plasma can penetrate up to 10 channel diameters upstream of the exit, depending on the flow rate of the vapor. Therefore, the minimum desired length is 10 diameters plus a distance that minimizes the thermal conduction to the cathode base.

Experimental results from two SCHCs are presented in the next section. Cathodes of different inner diameters (4 and 6 mm) demonstrate the diameter dependent effects. Smaller diameter cathodes could not be used because a hollow cathode discharge could not be produced with the flow rate range (0.2 to 50 mg/s) provided by our lithium feed system. The wall thickness was 0.5 mm.

2. MCHC Dimensions

The MCHC is constructed from a single piece of tungsten rod. Nineteen 1 mm channels were drilled in the end of the 10 mm diameter rod. The channels are 10 mm deep and open into a large volume upstream.

C. Lithium Evaporator

The evaporator has two functions; to evaporate lithium at a rate equal to the rate lithium flows into it and to provide a mount for the cathode. The lithium evaporator must operate at greater than 1100° C. The evaporator must conduct the power required for evaporation from the heater to a stable evaporation point. The material the evaporator is constructed from must possess a large enough thermal conductivity to maintain its temperature above the evaporation temperature, but not melt near the heater. Lithium has a high heat of evaporation (21200 kJ/kg or 21.2 W per mg/s), which is a large amount of power to deliver to the small evaporation point. Molybdenum was the best choice for the lithium evaporator material because it has a high melting temperature (2896 K), a high thermal conductivity (139 $\mathrm{Wm^{-1}K^{-1}}$), and can be machined with standard techniques.

The temperature is maintained by a graphite heater that is located within the evaporator. Our experience with graphite radiative heaters and the limited availability of resistive heaters that operate above 1100° C led us to use a 1.5 kW graphite heater.

D. Optical Access

Because lithium condenses on all surfaces below 1100°C, it is particularly difficult to maintain optical access through the view ports. Two methods were employed to combat lithium deposition on optical ports: 1) A film of mylar placed inside the facility, near the optical port is continually replaced with new film and 2) an argon gas barrier is located within the volume in front of the port.

Method 1 is called the *continuous-film* method. The concept was based on the tear-away plastic coverings that NASCAR drivers wear on their visors. The film was selected based on its ability to survive contact with lithium vapor and transmit optical wavelengths. Measurements with a spectrometer demonstrated that the light (300 to 850 nm) was uniformly transmitted through the mylar. A large sheet of film is used, the short dimension is just wider than the optical port diameter (6"). The long dimension is determined by how much film can be wrapped around the spool that holds it. For the present design, that is about 50'. The un-used film is pulled from one spool onto a second spool that is connected to a DC motor. The rate of the film travel is determined by the voltage applied to the motor. We determine lithium coverage by visual inspection and adjust the speed as necessary. Normally, the lowest possible rate of film motion is sufficient to limit lithium coverage.

Method 2, or the argon gas barrier method, works by blocking the flux of lithium toward the view port through collisions with argon gas. A volume of relatively high pressure argon is located along the optical path inside the facility. The view port is one end of the volume and an opening just large enough to allow full view of the experiment is at the other end (3 cm diameter). The argon carries the lithium from the volume and nearly eliminates the lithium coating on the view port.

V. Diagnostics

The diagnostics measure the most important discharge properties predicted by the cathode theories: the cathode temperature, plasma penetration depth, and the cathode voltage. Measurement of the cathode temperature profile with the multi-color video pyrometer gives both the temperature and penetration depth. To determine the cathode voltage, the plasma potential near the cathode tip must be measured. This requires measuring both floating potential and electron temperature at that location. The floating potential is measured with a Langmuir probe and the electron temperature is measured by emission spectroscopy.

A. Multi-color Video Pyrometry

The multi-color video pyrometer (MCVP) is a diagnostic developed at EPPDyL to measure the temperature of hot surfaces.[17] The MCVP records the radiated intensity of a surface at four wavelengths (404.7 nm, 514.5 nm, 632.8 nm, and 694.3 nm) on a single CCD. Utilizing a CCD to record the radiation allows the temperature to be determined over the entire surface. To reduce the error in intensity measurements, the intensity from ten images is included in the temperature determination routine. This technique is valid because the experiments were steady-state. The ±50°C uncertainty of the temperature is dominated by limitations of the calibration equipment.

B. Langmuir Probe

A Langmuir probe was utilized to measure the plasma floating potential near the cathode tip. The density was too great to measure the current as a function of voltage in the ion saturation region, so the electron temperature could not be determined with this probe. The Langmuir probe was a 0.01" tungsten wire with approximately 2 mm exposed to the plasma. The wire was insulated by a boron nitride tube. The voltage was recorded with an oscilloscope for 20 s at 250 samples per second at each data point. The floating potential was determined as the average of that data.

C. Emission Spectroscopy

The plasma electron temperature in the inter-electrode space, near the cathode, was measured utilizing emission spectroscopy. The spectrometer used in these observations is a Spex model 1702. This spectrometer features a 0.75 m focal length and a grating of 1200 grooves/mm, and is optimized for use in the visible (300 to 800 nm) range. The spectrometer grating is driven by a stepper motor, which is controlled by a Spex

CD2A Compudrive system consisting of a command keyboard and a drive controller. The camera used in these observations is a Princeton Instruments model ICCD-576 image-intensified CCD camera.

VI. Experimental Results and Discussion

The results from three different cathodes operating from 10 to 200 A and 0.2 to 1.6 mg/s are presented.

A. Experimental Procedure

A steady evaporation rate of lithium requires a stable evaporation point. To ensure the evaporation point had reached steady-state at each mass flow rate, the first 15 minutes of data after a mass flow rate adjustment was ignored. Also, the first 3 to 5 minutes after a current change was neglected.

B. Electron Temperature

The electron temperature was measured so that the plasma potential at the cathode tip, which is the cathode voltage V_c, could be determined. Using the floating potential, V_f, measurements and electron temperature, T_e, we find

$$V_c = V_f - \frac{kT_e}{e} \ln \left[4 \left(\frac{\pi m_e}{8 m_{li}} \right)^{1/2} \right], \tag{4}$$

where k is Boltzman's constant, e is the charge of an electron, and m_e and m_{li} are the masses of the electron and lithium atom, respectively. For a lithium plasma, the natural logarithm term is equal to -3.8. The measured electron temperature is between 0.2 and 0.7 eV and shows no strong correlations with the discharge parameters. The cathode potential measurement is calculated using the average electron temperature of 0.37 eV and a standard deviation of 0.12 eV without incurring more uncertainty than is associated with the floating potential data. Emission spectroscopy data were recorded for 20 different operating conditions with 4 different cathodes.

C. Cathode Temperature

The MCVP data was analyzed to determine the maximum temperature and the plasma penetration depth. The maximum temperature is shown in figures 5, 6, and 7. It is important to note that the maximum cathode temperature is independent of mass flow rate. The SCHC experimental results, shown in figures 5 and 6, indicate that at high current the maximum temperature increases weakly with current. The 4 mm and 6 mm cathodes operate at approximately 3000 K and 2800 K, respectively. The 6 mm cathode temperature has a stronger dependence on mass flow rate than the 4 mm one, which is due to the greater change in penetration depth (discussed below) and the concurrent greater change in density and ion impact heating of the cathode.

The MCHC experiment data indicate that the cathode temperature increases with current, as shown in figure 7. There is not a strong dependence on mass flow rate, but there is not a wide range of mass flow rate data to infer trends from.

The plasma penetration depth of the SCHCs is shown in figures 8, 9, and 10. A plasma penetration depth could not be determined in the MCHC experiment. The uncertainty is estimated to be 1 mm because the location of the cathode tip was determined by visual inspection in each case, but the data suggests a larger value would be more appropriate. The data from the 6 mm cathode is separated into two graphs to make the trends clearer. The penetration depth of the 0.8 mg/s, 6 mm cathode experiment does not follow a strong trend. The deviations are most likely due to changes in the mass flow rate provided by the lithium feed system.

Excluding the 0.8 mg/s, 6 mm cathode experiment, the penetration depth increases with current at a fixed mass flow rate. The penetration depth is also more sensitive to current at lower flow rates. This indicates that the arc requires more ions to impact the cathode surface and it is attaining them by increasing the area arc attachment area.

The MCHC did not have a measurable plasma penetration depth, which indicates that it could support a much higher current. This is obvious from the fact that each channel is conducting less than 10 A.

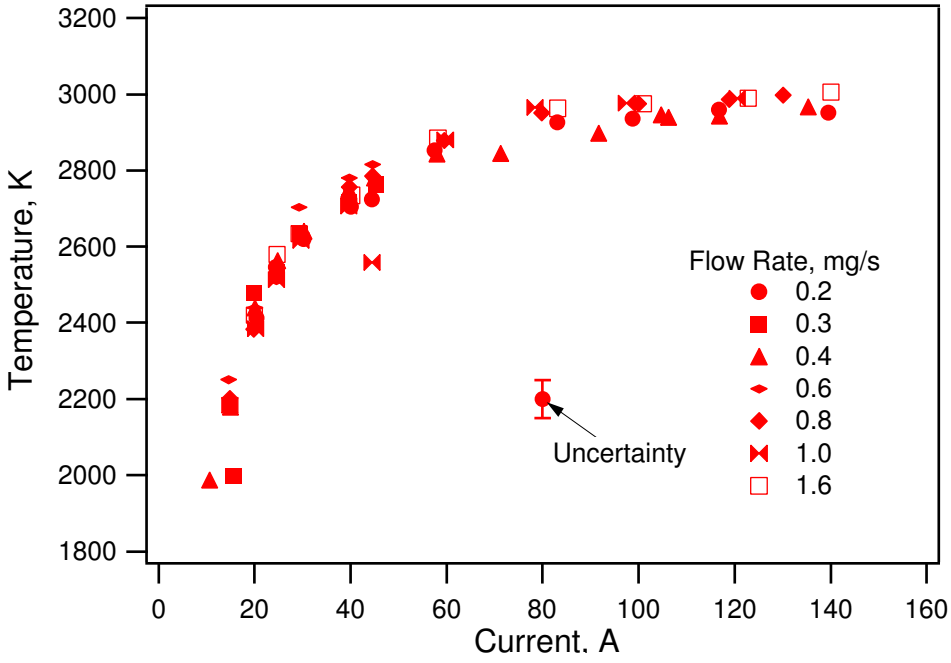

Figure 5. The maximum temperature of the 4 mm SCHC.

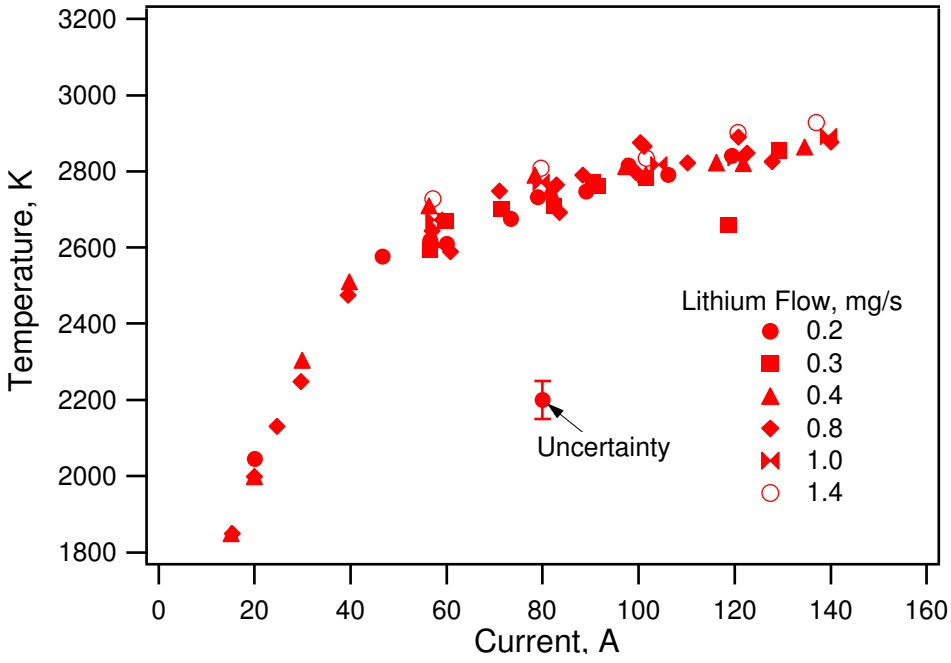

Figure 6. The maximum temperature of the 6 mm SCHC.

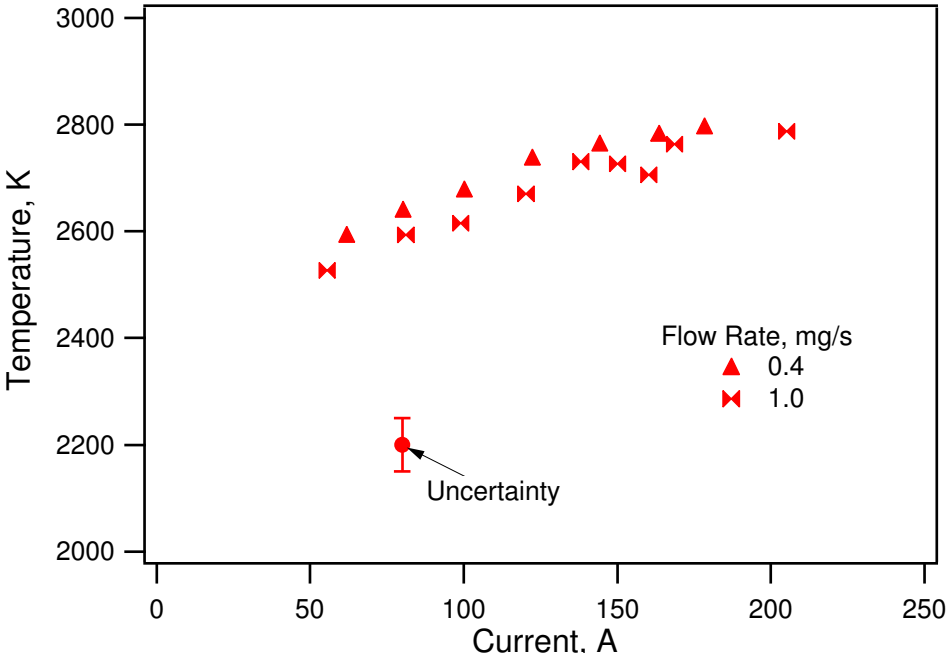

Figure 7. The maximum temperature of the MCHC.

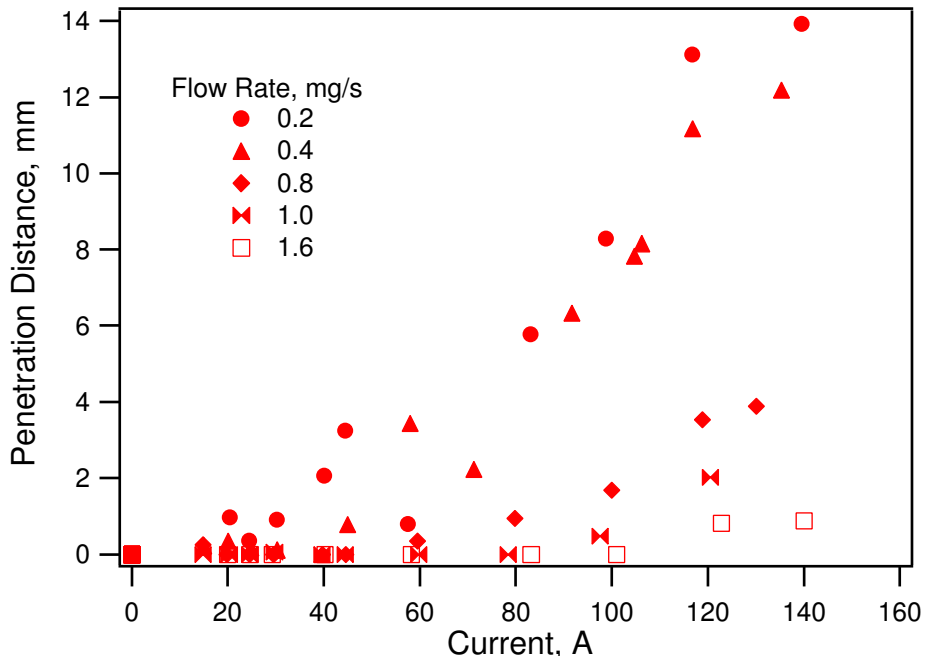

Figure 8. The location of the maximum temperature for the 4 mm cathode.

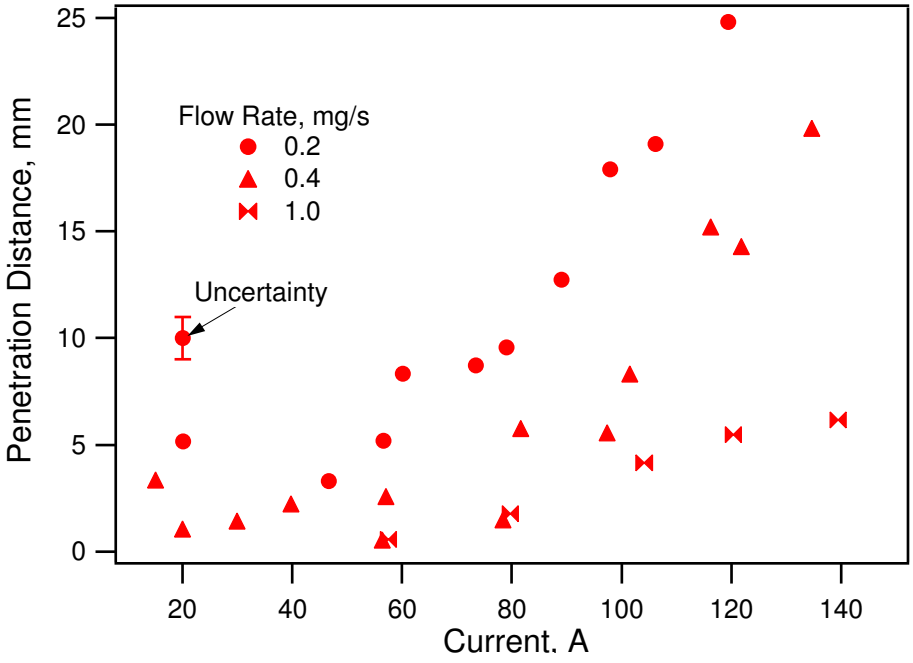

Figure 9. The location of the maximum temperature for the 6 mm cathode.

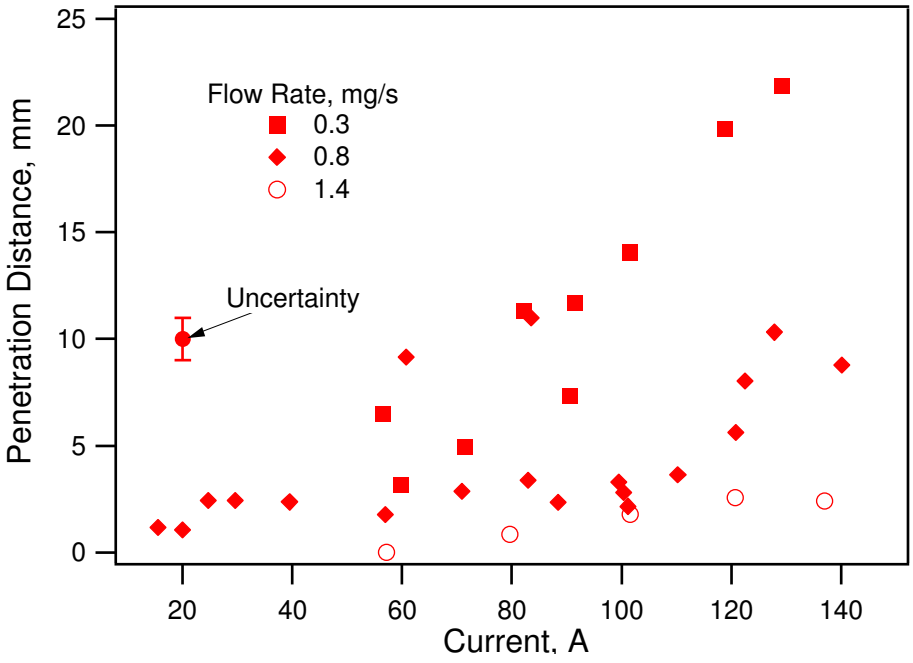

Figure 10. The location of the maximum temperature for the 6 mm cathode.

D. Cathode Voltage

The plasma potential approximately 3 mm downstream of the cathode tip was determined from the Langmuir probe floating potential and electron temperature measurements. The cathode voltage was taken to be the plasma potential because the electric field in the inter-electrode space was small. The results are shown in figures 11, 12, and 13.

The voltage decreases with current at currents greater than 30 A in the 4 mm SCHC experiment, shown in figure 11. At lower current, the trend is reversed. This is most likely due to a lithium coating on the cathode surface, which reduces the work function and therefore reduces the power required for thermionic emission. The voltage has a weak dependence on mass flow rate; the higher flow rates have slightly greater voltages. The plasma did not penetrate more than 2 mm for mass flow rates greater than 0.8 mg/s, which indicates that the cathode was operating in borderline hollow cathode mode. This effect could cause the increase in the voltage seen in the data.

The 6 mm SCHC experimental data, shown in figure 12, has similar trends in voltage as a function of current. There is no clear dependence on mass flow rate, most likely because the plasma penetrates the channel a measurable distance at every mass flow rate and current, as shown in figures 9 and 10. Plasma penetration allows the cathode to operate at the optimum voltage, which was measured to be nearly independent of mass flow rate.

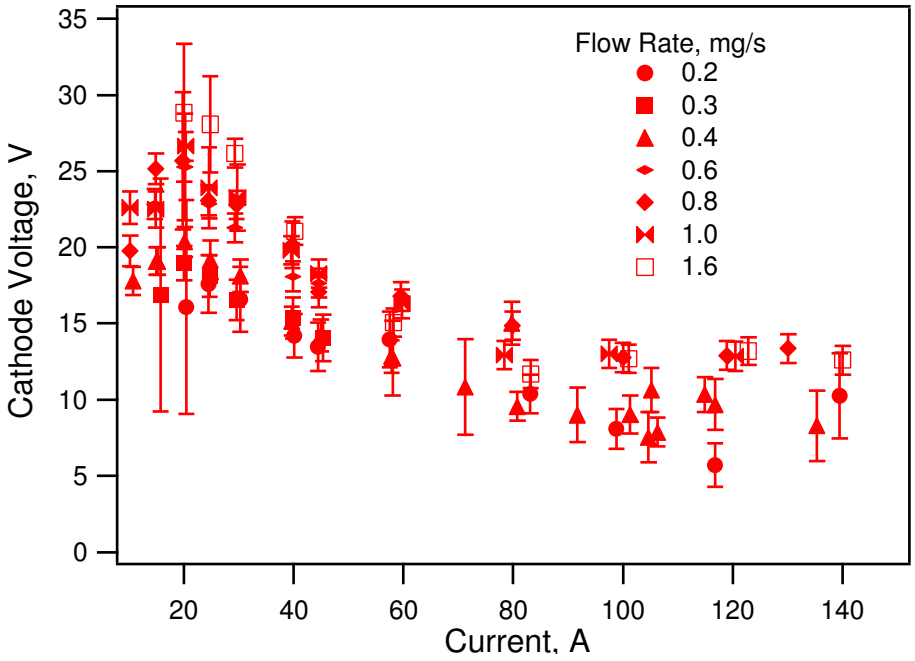

Figure 11. The cathode voltage of the 4 mm SCHC.

The voltage of the MCHC decreased with current throughout range of the experiment, as shown in figure 13. The voltage was also lower at a lower mass flow rate. Unfortunately, we do not have data at higher currents or lower mass flow rates to determine the optimum operational regime of this MCHC. The data do demonstrate that the MCHC does operate at a lower voltage than an SCHC when operating at similar currents and mass flow rates.

VII. Comparison with Theory

The results of the theory are compared to measurements of the 6 mm inner diameter SCHC to assess the validity of the model and to draw insight from the data. The measured and predicted temperatures of the cathode operating with 0.2 and 0.4 mg/s are shown in figure 14. The measured temperature is approximately 50 K lower than the internal surface temperature, which the SCHC model predicts. The temperature difference between the inner and outer surface is due to thermal conduction to the radiating external surface

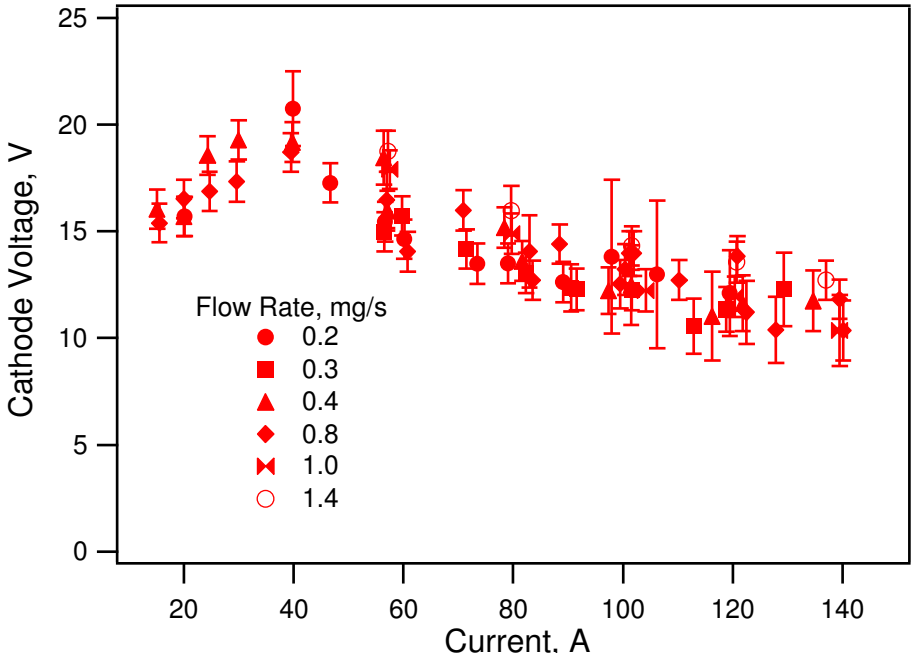

Figure 12. The cathode voltage of the 6 mm SCHC.

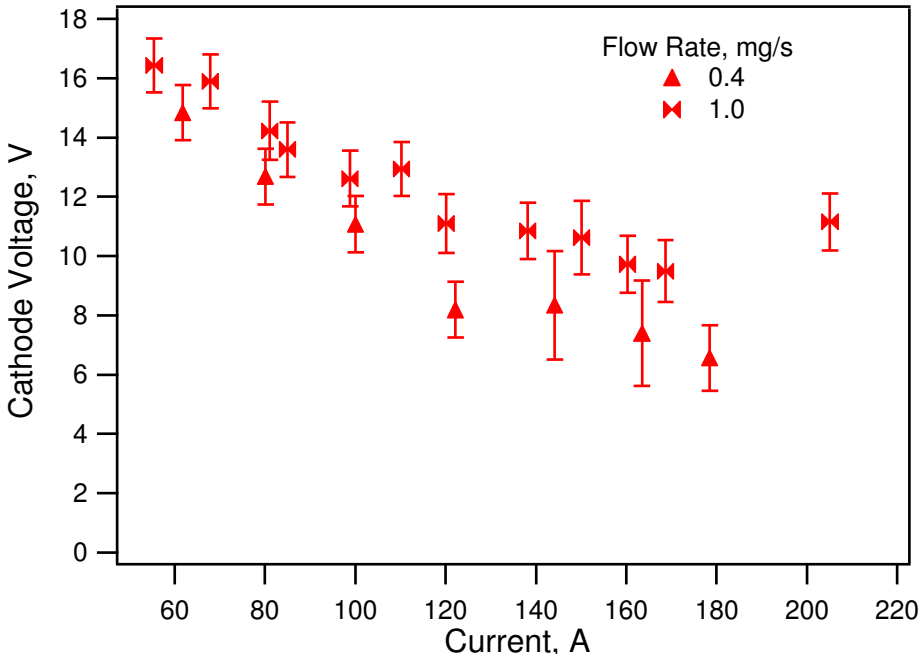

Figure 13. The cathode voltage of the MCHC.

through the cathode wall. At low and moderate current the theory over-predicts the temperature by 100 to 200 K. Some of this difference can be attributed to a lithium coating on the surface and the heat conducted along the cathode walls. At high current (>100 A), the predictions and measurements agree within the ±50 K error of the measurement.

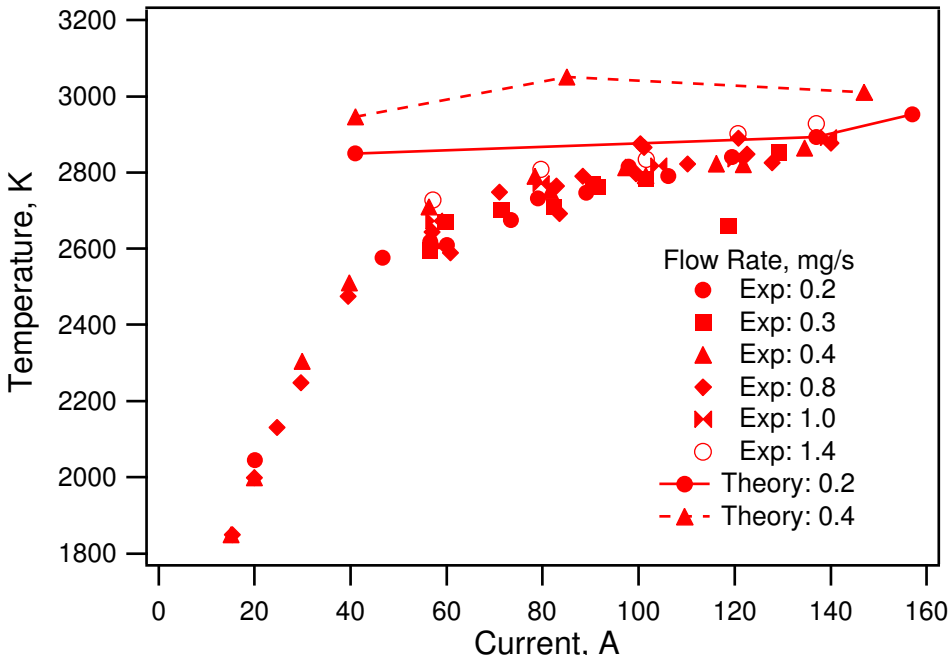

Figure 14. A comparison of the predicted and measured cathode temperature.

The plasma penetration depth compares less favorably, as shown in figure 15. The theory predicts the trends of an increasing penetration depth as a function of current and a deeper penetration with less mass flow rate. The difference between experiment and theory is that the predicted penetration depth is changes less with current than measured. This could be attributed to an inaccurate model of the pressure within the channel, and will be analyzed in the future.

The MCHC theory predicted the operating parameters for a 19 channel cathode (1 mm diameter) operating at 222 A with a mass flow rate of 1.0 mg/s. The voltage measured in our experiment was 11 V, compared to to 7 V predicted by the theory. The predicted temperature was 3150 K, compared to a measured 2800 K. The measured temperature is at least 100 K below the temperature within the channels, leaving a 250 K disparity.

The models also give insight into the operation of the cathodes. They predict that the plasma within the channel is fully ionized during high-current operation, and that the penetration depth is located at the point where the density can sustain the required current. Since, for a given channel radius, the total density increases with mass flow rate and distance upstream of the exit, both the experiments and theory predict a dependence of penetration depth on mass flow rate. The increase in penetration depth (hence density) with current is also explained by the requirement of a greater ion flux to heat the cathode surface for thermionic emission. Also, because the plasma density at the upstream attachment point is similar (even at different mass flow rates) the temperature and voltage of the cathode are also similar when operated at the same current.

VIII. Conclusions

We have presented theories for the single-channel and multichannel hollow cathodes that include the relevant physical processes. They predict the operating parameters of cathode voltage and temperature profile. The independent parameters of the model are current, lithium flow rate, channel diameter, and number of channels (in the case of the MCHC). The theories include, for the first time, a non-equilibrium

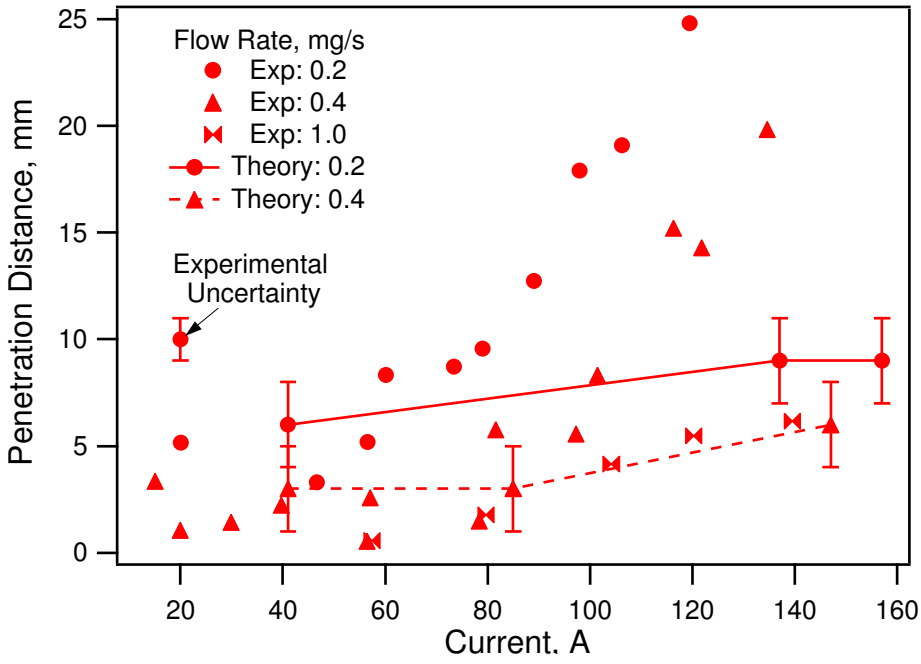

Figure 15. A comparison of the predicted and measured penetration depth.

excitation and ionization model of the working gas and a prediction of the plasma penetration depth.

We have also presented the design and results of lithium-fed hollow cathode experiments. The plasma penetration depth was shown to increase with current and decrease with mass flow rate. These results are reported for the first time. Experimental results also show that the SCHC temperature increases slightly and the voltage decreases slightly with current at conditions where there is plasma penetration.

This study was able to give insight into the dependencies of the plasma penetration depth, voltage, and cathode temperature on the operating parameters. The combination of theory and experiment was able to demonstrate that the penetration depth is determined by the location of a plasma density able to heat the cathode surface to the thermionic emission temperature required by the external circuit. Because the arc finds the location of optimal density, the cathode temperature and voltage are independent of mass flow rate (at a given current) and the penetration depth is dependent on both mass flow rate and current.

References

[1]Frisbee, R., "SP-100 Nuclear Electric Propulsion for Mars Cargo Missions," *29th AIAA/SAE/ASME/ASEE Joint Propulsion Conference*, Monterey, CA, USA, June 1993, AIAA-93-2092.

[2]Frisbee, R., "Electric Propulsion Options for Mars Cargo Missions," *32nd AIAA/ASME/SAE/ASEE Joint Propulsion Conference and Exhibit*, Lake Buena Vista, FL, USA, July 1996, AIAA-96-3173.

[3]Polk, J., "Alkali Metal Propellants for MPD Thrusters," *AIAA/NASA/OAI Conference on Advanced SEI Technologies*, Cleveland, OH, USA, September 1991, AIAA-91-3572.

[4]Sankaran, K., Cassady, L., Kodys, A., and Choueiri, E., "A Survey of Propulsion Options for Cargo and Piloted Missions to Mars," *Astrodynamics Space Missions and Chaos*, edited by E. Belbruno, D. Folta, and P. Gurfil, Vol. 1017, Annals of the New York Academy of Sciences, New York, NY, USA, 2004, pp. 450–567.

[5]Ageyev, V., Ostrovsky, V., and Petrosov, V., "High-current Stationary Plasma Accelerator of High Power," *23rd International Electric Propulsion Conference*, AIAA/AIDAA/DGLR/JSASS, Seattle, WA, USA, September 1993, pp. 1071–1075, IEPC-93-117.

[6]Delcroix, J., Minoo, H., and Trindade, A., "Gas Fed Multichannel Hollow Cathode Arcs," *Review of Scientific Instruments*, Vol. 40, No. 12, December 1969, pp. 1555–1562.

[7]Ferreira, C. and Delcroix, J., "Theory of the Hollow Cathode Arc," *Journal of Applied Physics*, Vol. 49, No. 4, April 1978, pp. 2380–2395.

[8]Babkin, G., Mikhalev, V., Ogorodnikov, S., Orlov, R., and Potapov, A., "High-current Coaxial Plasma Source," *Soviet Physics - Technical Physics*, Vol. 20, No. 9, 1976, pp. 1175–1178.

[9]Babkin, G., Mikhalev, V., Morozov, E., and Potapov, A., "An Experimental Investigation of a Plasma in a Multichannel Cathode," *Journal of Applied Mechanics and Technical Physics*, Vol. 17, No. 6, 1976, pp. 767–770.

[10]Grishin, S., Litvak, A., Ogorodnikov, S., and Stepanov, V., "Intermediate-power Steady-state Plasma Accelerator," *Soviet Physics - Technical Physics*, Vol. 22, No. 2, February 1977, pp. 280–285.

[11]Fradkin, D., Blackstock, A., Roehling, D., Stratton, T., Williams, M., and Liewer, K., "Experiments Using a 25 kW Hollow Cathode Lithium Vapor MPD Arcjet," *AIAA Journal*, Vol. 8, No. 5, May 1970, pp. 886–894.

[12]Ageyev, L., Grishin, S., Mikhalev, V., Ogorodnikov, S., and Stepanov, V., "Characteristics of High-current Plasma Sources with a Hollow Cathode," *Radio Engineering and Electronic Physics-USSR*, Vol. 20, No. 9, 1975, pp. 67–71.

[13]Cassady, L. and Choueiri, E., "Lithium-Fed Hollow Cathode Theory," *40th AIAA/ASME/SAE/ASEE Joint Propulsion Conference and Exhibit*, Ft. Lauderdale, FL, USA, July 2004, AIAA-2004-3431.

[14]Ogarkov, V., Ogorodnikov, S., and Stepanov, V., "The Design of the Multirod Cathode of a High-current Plasma Source," *Radio Engineering and Electronic Physics-USSR*, Vol. 21, No. 12, 1976, pp. 98–103.

[15]Ogarkov, V., Ogorodnikov, S., and Stepanov, V., "The influence Adsorption Effects on the Characteristics of a High-current Multirod Cathode," *Radio Engineering and Electronic Physics-USSR*, Vol. 23, No. 8, 1979, pp. 123–127.

[16]Kodys, A., Emsellem, G., Cassady, L., Polk, J., and Choueiri, E., "Lithium Mass Flow Control for High Power Lorentz Force Accelerators," *Space Technology and Applications International Forum*, Albuquerque, NM, USA, February 2001, STAIF Paper 195.

[17]Cassady, L. and Choueiri, E., "High Accuracy Least-squares Multiple-color Pyrometry for High Temperature Surfaces," *28th International Electric Propulsion Conference*, Tolouse, France, March 2003.